Remote Sensing of Environment 249 (2020) 112010

Contents lists available at ScienceDirect

Remote Sensing of Environment

journal homepage: www.elsevier.com/locate/rse

Half a century of forest cover change along the Latvian-Russian border captured by object-based image analysis of Corona and Landsat TM/OLI data

Zigmars Rendenieks[a,c], Mihai D. Nita[a,b], Oļģerts Nikodemus[c], Volker C. Radeloff[a,*]

[a] SILVIS Lab, Department of Forest and Wildlife Ecology, University of Wisconsin-Madison, 1630 Linden Drive, Madison, WI 53706, USA
[b] Department of Forest Engineering, Faculty of Silviculture and Forest Engineering, Transilvania University of Brasov, 1 Sirul Beethoven, Brasov, Romania
[c] Department of Geography and Earth Sciences, University of Latvia, Jelgavas iela 1, Riga LV-1004, Latvia

ARTICLE INFO

Keywords:
Afforestation
Agricultural land abandonment
Corona imagery
Forest mapping
Latvia
Satellite images
Remote sensing
Russia

ABSTRACT

After 1991, major events, such as the collapse of socialism and the transition to market economies, caused land use change across the former USSR and affected forests in particular. However, major land use changes may have occurred already during Soviet rule, but those are largely unknown and difficult to map for large areas because 30-m Landsat data is not available prior to the 1980s. Our goal was to analyze the rates and determinants of forest cover change from 1967 to 2015 along the Latvian-Russian border, and to develop an object-based image analysis approach to compare forest cover based on declassified Corona spy satellite images from 1967 with that derived from Landsat 5 TM and Landsat 8 OLI images from 1989/1990 and 2014/2015. We applied Structure-from-Motion photogrammetry to orthorectify and mosaic the scanned Corona images, and extracted forest cover from Corona and Landsat mosaics using object-based image analysis in eCognition and expert classification. In a sensitivity analysis, we tested how the scale parameters for the segmentation affected the accuracy of the change maps. We analyzed forest cover and forest patterns for our full study area of 22,209 km^2, and applied propensity score matching approach to identify three Latvian-Russian pairs of 15 × 15 km cells, which we compared. We attained overall classification accuracies of 92% (Latvia) and 93% (Russia) for the forest/non-forest change maps of 1967–1989, and 91% (Latvia) and 93% (Russia) for 1989–2015, and our results were robust in regards to the segmentation scale parameter. Sample-based forest cover gain from 1967 to 1989 differed notably between the two countries (18.5% in Latvia and 23.6% in Russia), but was generally much higher prior to 1989 than from 1989 to 2015 (8.7% in Latvia and 9.7% in Russia). Furthermore, we found rapid de-fragmentation of forest cover, where forest core area increased, and proportions of isolated patches and forest corridors decreased, and this was particularly pronounced in Russia. Our findings highlight the need to study Soviet-time land cover and land use change, because rural population declines and major policy decisions such as the collectivization of agricultural production, merging of farmlands and agricultural mechanization led already during Soviet rule to widespread abandonment and afforestation of remote farmlands. After 1991, government subsidies for farming declined rapidly in both countries, but in Latvia, new financial aid from the EU became available after 2001. In contrast, remoteness, lower population density, and less of a legacy of intensive cultivation resulted in higher rates of forest gain in Russia. Including Corona imagery in our object-based image analysis workflow allowed us to examine half a century of forest cover changes, and that resulted in surprising findings, most notably that forest area gains on abandoned farm fields were already widespread during the Soviet era and not just a post-socialist land use change trend as had been previously reported.

1. Introduction

After the collapse of the USSR in 1991, post-Soviet Eastern Europe experienced dramatic land use and land cover change (Gutman and Radeloff, 2017; Kuemmerle et al., 2016), which was predominantly caused by the transition from planned to market economies (Mathijs and Swinnen, 1998). One major result of this transition was widespread farmland abandonment due to the reforms in the agricultural sector, weaker institutions, decreased subsidies, land privatization, and loss of guaranteed markets (Ioffe et al., 2012, 2004; Lerman et al., 2004).

* Corresponding author.
E-mail address: radeloff@wisc.edu (V.C. Radeloff).

https://doi.org/10.1016/j.rse.2020.112010
Received 18 July 2019; Received in revised form 2 July 2020; Accepted 18 July 2020
Available online 04 August 2020
0034-4257/

These major changes accelerated the effects of decades-long population declines in rural Russia (Ioffe et al., 2012). Farmland abandonment, in turn, resulted in forest area increases due to natural succession (Kuemmerle et al., 2011; Potapov et al., 2015), albeit with considerable time lags the length of which depended on local biophysical conditions (Bartha et al., 2003; Ruskule et al., 2012). However, while post-Soviet abandonment is well documented, it is largely unclear how much abandonment occurred already during Soviet times, and if post-socialist abandonment was novel, or merely the continuation of long-term trends (Kuemmerle et al., 2015).

Unfortunately, there is relatively little information on land use change in Eastern Europe during Soviet rule, largely due to the lack of spatially explicit data. There are reports of abandonment of more remote and less productive croplands and pastures already after soviet collectivization of agricultural lands and rural populations (Nikodemus et al., 2005). However, while collectivization in Russia occurred in the 1920s, Latvia was an independent country before WW II, with a market economy, fast developing agricultural sector, and state-dominated forestry. Even after Latvia become part of the Soviet Union, it had higher level of mechanization and agricultural yields than Russia (Lerman et al., 2004). Across the Soviet Union though, a new wave of intensification of agricultural production started in mid-1960s, making some areas in turn marginal for agriculture, causing abandonment (Boruks, 2003). Especially in regions where traditional rural population structure consisted of spatially scattered farmsteads, such as Latvia's hilly uplands, the effects of collectivization was stark (Grīne, 2009; Penēze, 2009). Later, in the 2000s, strong outmigration and aging rural populations contributed to the abandonment of agricultural lands (Bell et al., 2009).

Studies of farmland abandonment in the former Soviet Union and Eastern Europe, have largely focused on the era after the mid-1980s, because this is when the first 30-m Landsat data became available. The problem is that 30-m data from Landsat covers only the final years of the Soviet Union, and are hence insufficient to assess land use change during Soviet time, as well as legacies of socialist land use on land use change after the collapse (Munteanu et al., 2017). Landsat MSS data is available for the 1970s already, but spatially too coarse (60-m) to map farmland accurately in Eastern Europe. High-resolution Corona imagery is a unique data source, providing valuable information on land cover in the 1960s, almost two decades prior to 30-m Landsat data. Corona data has a great potential for detailed mapping of environmental conditions, thus enabling long-term studies (McDonald, 1995; Song et al., 2015). Designed for military reconnaissance and mapping purposes, Corona imagery is still rarely utilized in land use and land cover change research (Nita et al., 2018; Rigina, 2003; Song et al., 2015; Tappan et al., 2000), despite the fact that it was already declassified in 1995.

So far, only a handful of studies have conduct change analyses based on the combination of Corona and Landsat data. The earliest was by Lorenz (2004), who georeferenced several KH-4A strips to a Landsat 5 TM image to digitize geological structures. Bolch et al. (2008) analyzed four Corona KH-4A image strips, in conjunction with Landsat 5 TM and ASTER images to study glacier changes. They geo-registered Corona strips to a thematic map and used ASTER Digital Elevation Model (DEM) to rectify Corona and ASTER images with a Root Mean Square Error (RMSE) of < 20 m and < 30 m, respectively. The first study to map forest changes based on georeferenced Corona images to Landsat 7 images was performed by Song et al. (2015), who calculated texture metrics based on the spectral heterogeneity surrounding each pixel, and applied a Support Vector Machine (SVM) classifier to map forested area change at the pixel-level in both the eastern US and in Brazil. Image texture also improved land cover classifications from Corona and Landsat MSS data in China (Shahtahmassebi et al., 2017). These studies made important contributions, and highlighted the potential for long-term change analyses based on Corona and Landsat data, which makes it all the more surprising that such analyses are not more common yet.

We suggest that there are two main reasons why Corona data has not seen wider use. First, the imagery is difficult to geo-rectify (Sohn et al., 2004; Song et al., 2015), and, second, it is difficult to map land cover automatically for large areas from Corona data. Recently, Nita et al. (2018) developed new methods to georectify Corona imagery accurately based on approaches that are based on Structure from Motion, and demonstrated the feasibility to accurately georectify Corona imagery for large areas by analyzing all of Romanian Carpathian forests. However, the automated mapping of land cover from Corona imagery, and the analysis of time series of Corona and Landsat imagery remains difficult because the spatial and radiometric resolution of the two types of data is so different. This is the methodological challenge that we sought to overcome here. Specifically, we opted to apply object-based image analysis to both Corona and Landsat data to facilitate change analyses. Object-based image analysis can extract features from high-resolution images (Blaschke, 2010; Hossain and Chen, 2019) and is well suited for Corona data given their limited spectral information and inherent noise (Gheyle et al., 2011; Gurjar and Tare, 2019).

Our goal was to analyze the rates and determinants of forest cover change from 1967 to 2015 along the Latvian-Russian border. We had two specific objectives: (1) to map and quantify forest cover change from 1967 to 2015 from Corona and Landsat imagery using based on object-based imagery analysis, and (2) analyze the influence of the segmentation scale parameter in the object-based image analysis of Corona and Landsat imagery on the accuracy of forest cover change maps.

2. Methods

2.1. Study area

Our study encompasses 175 km of the Latvian-Russian border (Fig. 1) and included parts of Eastern Latvia and Russia. The total area is 22,209 km^2, the approximate size of a 150 × 150 km square (i.e., slightly smaller than one Landsat footprint). 35.4% of the study area (7839 km^2) is in Latvia and 64.6% (14,370 km^2) in Russia's Pskov district. Hereafter, we use the names “Latvian SSR” and “Latvia” (before and after 1991) as well as “Russian SFSR” and “Russia” (before and after 1991) to refer to the portions of both countries covered by our study area.

The terrain of the study area consists of rolling glacial uplands in the southern part and the Velikaya lowland in the central and northern parts. Elevation ranges from 60 to 230 m a.s.l. Climate is cool temperate with mean temperatures of −3.6 °C in January and +17.4 °C in July, and annual precipitation is 709 mm (Nikodemus et al., 2018). Our study area is part of the hemiboreal biome and dominated by temperate coniferous, mixed and deciduous forests. Dominant tree species are Silver birch *Betula pendula*, Norway spruce *Picea abies* and Scots pine *Pinus sylvestris*, mostly in mixed stands. Most of the upland and hilly areas are covered by spruce-dominated forests (Nikodemus et al., 2018). Population density in 2015 was 7.6 people/km^2 in Russia and 13.6 people/km^2 in Latvia (Central Bureau of Statistics, 2018; ROSSTAT 2015). Dominant soil types are Luvisols, Retisols, Stagnosols, Gleysols and Podzols (Jones et al., 2005), which were formed on glacial, glaciolimnic and aeolian sediments. Bogs and swamps cover large areas at lower elevations.

Our entire study area was a part of the Soviet Union until 1991 when Latvia regained its independence. Although very similar biophysically, both sides of the border have different land use histories and patterns.

The Russian part of the study area covers the south of Pskov oblast. Pskov has long history of agriculture and forestry, mostly to supply local markets (Angelstam and Dönz-Breuss, 2004). The agricultural sector is dominated by dairy farming (ROSSTAT, 2015). The area is considered sub-marginal for agriculture due to low soil fertility and long distances to the district's center (Ioffe et al., 2006). As of 2011, 38% of Pskov oblast was covered with forests (Chabak, 2011).

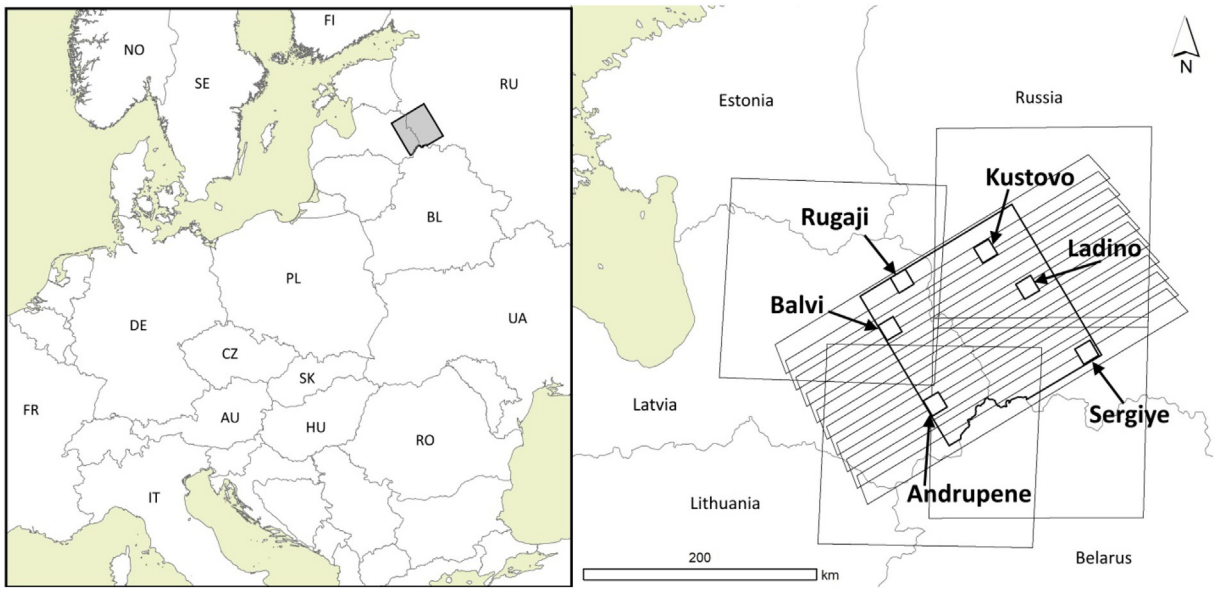

Fig. 1. Location of our study area in Europe, and the locations of Corona and Landsat footprints and six selected 15 × 15 km focal cells inside the study area.

The Eastern Latvian rural landscape prior to Soviet rule consisted of a mosaic of fields, meadows, lakes and separate farmsteads, but this changed dramatically after WW II due to the forced collectivization of cultivated lands under Soviet rule (Melluma, 1994). However, the first kolkhoz in Latvia was established almost twenty years later (1946) than in Russia (1928). During the Soviet period, eighty-five collective farms were located inside the Latvian section of our study area (Turlajs, 1998), all of them in districts that are considered "Less favored areas for cultivation" and which exhibit negative long-term socio-economic trends (Cabinet of Ministers, 2006).

Within our study area, we analyzed six 15 × 15 km focal cells in detail – three in Latvia and three in Russia and named each after the closest populated place: in Latvia – Rugaji, Balvi and Andrupene; in Russia – Kustovo, Ladino and Sergiye. These focal cells varied in proportions and patterns of forest cover, as well as in distance to closest town or city, representing a range of variability in terms of land cover composition and forest patterns.

2.2. Data

We analyzed two types of satellite images: historic images from Corona missions, and Landsat 5 and 8 images (Table 1). Corona was a reconnaissance program that included Corona, Argon and Lanyard spy satellites, and was operated by the U.S. from 1960 to 1972 (McDonald, 1995). Declassified in 1995, images from Corona satellites provide information on land surface conditions, including forest cover in the mid-1960s (Fig. 2). We purchased 18 panchromatic cloudless Corona (KH-4B) mission 1101 scanned film images recorded on September 16th 1967 from the USGS archive (https://earthexplorer.usgs.gov/). We selected these images because of their superb quality. They are the earliest cloudless scenes taken by the most advanced sensor from all Corona missions (Song et al., 2015). The original resolution of the scanned film images was 7 μm (Table 2). The images that we analyzed were nine adjacent stereo pairs (see Fig. 1). The dimensions of each strip (footprint) are approximately 15 × 252 km, and each strip is cut in four segments. These images are panoramic, and so we analyzed only the two central segments (middle half) of the strip, because they are closer to nadir and less distorted. Corona images contain several types of distortions, all of which are more acute at the ends of the image strip. Oblique angle of exposure and conical projection produces image displacements and increases the area captured by one pixel. Panoramic distortion is due to rotating cameras. S-shaped distortion occurs due to the movement of satellite sensor at the moment of image capture. Image motion compensation onboard the satellite was used to reduce S-shaped distortion, but did not fully eliminate it. Other distortions are related to the curvature of Earth, camera tilt and unpredictable movement of the satellite (Goossens et al., 2006; Scollar et al., 2016). We performed no atmospheric correction for the Corona images because such correction would not affect our classifications. We also analyzed four Landsat 5 (TM) images and four Landsat 8 (OLI) images (Table 1). Landsat (initially – ERTS) is a program of multispectral Earth-observation satellites, that has been operated by the U.S. since 1972 (Lauer et al., 1997; Wulder et al., 2019). We selected these Landsat TM images because they were from 1989 to 1991, i.e., roughly at the midpoint 1967 to 2015, and right at the collapse of the Soviet Union, and because they were cloud free. All data was downloaded as surface reflectance Level-2 images (LEDAPS and LaSRC corrected) from the USGS Science Research and Development (LSRD) service (https://espa.cr.usgs.gov/index/).

Furthermore, we included forest cover data from Potapov et al. (2015) to aid classification of forest objects, and to calculate the area affected by forest loss (see Discussion). Lastly, we used NASA Shuttle Radar Topography Mission 30 arc-second DEM tiles in support of the orthorectification of the Corona images.

2.3. Preprocessing of satellite images

Because we obtained the Corona images as scanned film, they required considerable amount of preprocessing. We stitched the fragments of scanned film together with Image Composite Editor and created one file from the two central segments of each panoramic image. To orthorectify the scanned Corona images, we applied a Structure-from-Motion (SfM) photogrammetry workflow in Agisoft PhotoScan Pro 1.2 (following Nita et al., 2018). In this workflow, the software: (1) finds tie points (pixels, which are identifiable in both images) automatically; and (2) aligns two images, reconstructing the positions of the satellite instrument at the moment of image recording. After successful alignment of images, (3) the software generates a dense point cloud, and a digital surface model. To improve the accuracy of the orthorectification and fill gaps in the data, we substituted the DSMs derived from dense point clouds with SRTM data. After this, (4) we georeferenced the dense point cloud with 14–16 user-provided ground control points (GCPs), (5) orthorectified images using the SRTM surface model, and (6) produced an orthomosaic of all the images. The spatial

Table 1
The list and characteristics of the image data that we analyzed.

Platform, sensor	Type	Date	Footprints	Spatial resolution	Encoding
Corona KH-4B (Mural)	Scanned film, stereo pairs	9/16/1967	DS1101-1009DA023, DS1101-1009DA024, DS1101-1009DA025, DS1101-1009DA026, DS1101-1009DA027, DS1101-1009DA028, DS1101-1009DA029, DS1101-1009DA030, DS1101-1009DA031, DS1101-1009DF016, DS1101-1009DF017, DS1101-1009DF018, DS1101-1009DF019, DS1101-1009DF020, DS1101-1009DF021, DS1101-1009DF022, DS1101-1009DF023, DS1101-1009DF024	2.53 m	8-bit unsigned integer
Landsat 5 (TM)	L-2A product	7/6/1989 7/8/1989 5/6/1990	186–21 184–20, 21 185–20	30 m	16-bit unsigned integer
Landsat 8 (OLI)	L-2A product	8/7/2014, 8/8/2015	185–20, 185–21 183–20, 183–21	30 m	16-bit unsigned integer

resolution of the resulting orthomosaic for Corona was 2.53 m. Aggregate horizontal (x,y) geo-registration error for the Corona orthomosaic was equivalent to one Landsat image pixel (31.06 m). That level of misregistration could have affected our subsequent change analysis, which is why we georeferenced the final orthomosaic to the Landsat 8 mosaic (sensu Song et al., 2015) in ArcMap using a third-order polynomial transformation to minimize the effects of any co-registration differences on the change analyses. For this, we used 51 evenly distributed road crossings and buildings as GCPs, and 17 random validation points. The co-registration to the Landsat imagery reduced the final geolocation error to 11.3 m. We chose Nearest Neighbor as our resampling algorithm, because it does not introduce new values in image, and the image was intended to use for classification.

To analyze land cover in 1989 and 2015, we mosaicked the 30-m bands from four Landsat 5 (bands 1, 2 and 3) and four Landsat 8 (bands 2, 3 and 4) footprints with ENVI 5.2. All three image mosaics (1967, 1989, and 2015) were cropped to match our study area.

2.4. Object-based image analysis and expert classification

We mapped forest cover from both Corona and Landsat images using Object Based Image Analysis, implemented as Multiresolution segmentation algorithm in eCognition Developer© 9.3 (Trimble, 2018). We chose an object-based approach, rather than a pixel-based approach, because of the high level of noise in Corona images in forms of graininess, haze, and scanning artifacts (Dashora et al., 2007). We set the scale parameter to 50 for the segmentation of both Corona and Landsat mosaics. “Scale parameter” here denotes a software-specific heterogeneity threshold used in the image object delineation (Benz et al., 2004). We used object based image analysis to delineate forest and non-forest objects, and did not intend to match object size with the average size of forest stands or tracts delineated for management purposes. The total number of image objects for 1967 map was 2,210,424 (837,591 in Latvia and 1,372,833 in Russia); for 1989 map it was 365,162 (150,672 in Latvia and 214,490 in Russia) and for 2015 map the total number was 413,305 (177,097 in Latvia and 236,208 in Russia).

We conducted a supervised classification to classify each image object as ‘forest’ or ‘non-forest’. We assigned objects to the category ‘forest’ based on visual assessments of segments that were predominantly covered with trees. Once the Corona images were classified, we resampled the classification to 30 m to match Landsat's resolution using Nearest Neighbor resampling in ENVI. Furthermore, we set the minimum mapping unit for the classified forest maps to 1 ha for both Corona and Landsat data. Objects below this threshold were merged with the surrounding class (i.e., forest or non-forest). Based on the classification for 1967, 1989, and 2015, we generated maps of forest change for 1967–1989, and for 1989–2015 based on post-classification comparisons.

2.5. Validation and accuracy assessment

Because we classified image objects, not pixels, image objects (i.e., polygons with a minimum size of 1 ha) were also the sample unit of analysis for our accuracy assessment. We performed the accuracy assessment for four change maps, and for each of the four classes: ‘stable forest’, ‘stable non-forest’, ‘forest gain’, and ‘forest loss'. For validation, we split our wall-to-wall change maps into their Latvian and Russian parts, in order to compare accuracy in both parts, and to estimate areas accurately in each. For validation, we used stratified random sampling (Olofsson et al., 2014, 2013) with 300 image objects for entire study area: 90 for stable forest and stable non-forest classes and 60 for forest gain and forest loss classes. We randomly selected sample polygons from the list of polygon IDs. Since we split wall-to-wall change maps, the number of samples in countries is different. Due to the absence of independent reliable reference data that depicted the situation close to

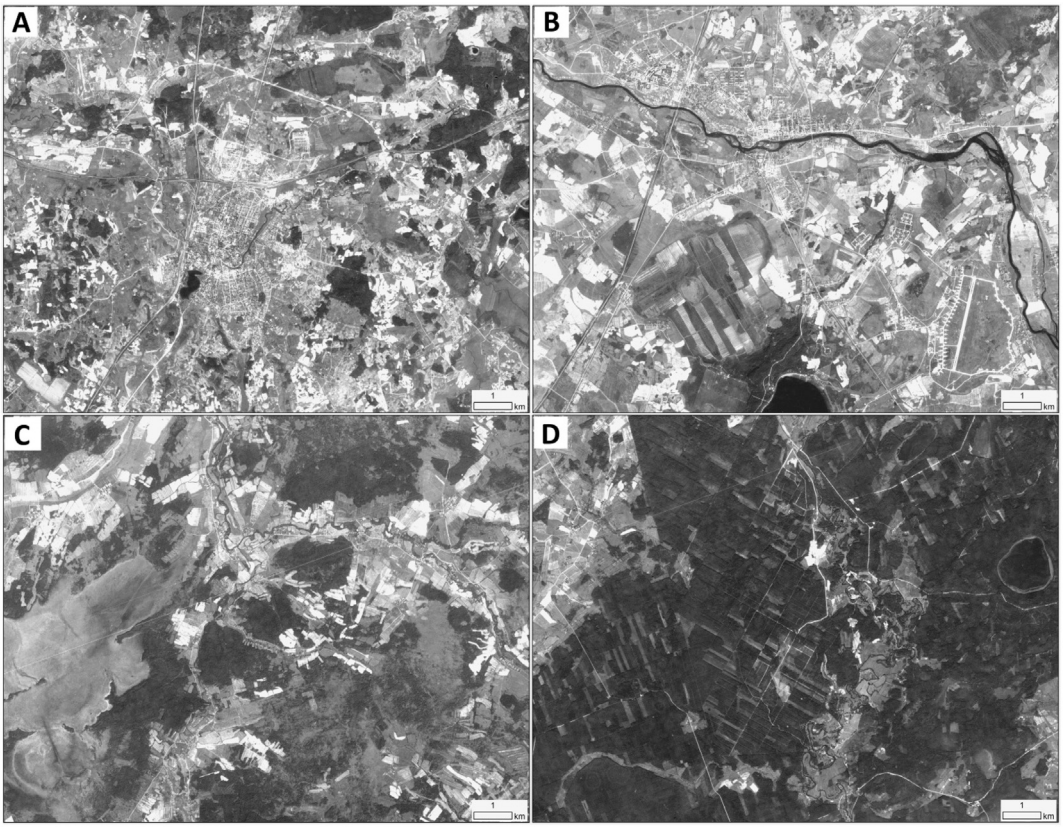

Fig. 2. Examples of Corona photographs from our study area (recorded on September 16th 1967): (A) city of Rēzekne, with the largest population inside our study area; (B) city of Ostrov, the largest in Russian part; (C) villages and abandoned fields NE from Ostrov (Russia); (D) logging pattern in forest tract NW of Rēzekne (Latvia).

Table 2
Properties of the Corona KH-4B images (Galiatsatos, 2009; Galiatsatos et al., 2007; National Reconnaissance Office, 1967).

Sensor type	KH-4B
Period of operation	9/15/67–5/25/72
Camera type	Panoramic, panchromatic
Camera model	J-1 Mural
Lens	F/3.5 Petzval
Film type	Petzval Type II
Film spectral range	500–680 μm
Focal length	606.9 mm
Film size	757 mm × 70 mm
Orbital altitude	150 km (lowest)
Scanning angle	71.16° (across track)
Field of view	5° (along track)
Nominal ground area	15 × 252 km
Film resolution	7 μm (scanned)
Nominal film photoscale	1: 247,500
Ground resolution	1.8–7.60 m

the investigated dates (e.g., we did not have access to aerial photographs for 1989, and Google Earth does not provide high-resolution imagery for that date), we examined the original Landsat 5 mosaic as our reference for 1989, combined with a Sentinel-2 10 m image mosaic from 8/8/2015 as reference data for the 1989–2015 change map. Similarly, we used the source data (Corona mosaic and the Landsat 5 mosaic) for the 1967–1989 change map. We interpreted the imagery visually and assigned the class value to each validation polygons based on the majority of pixels within that polygon. We calculated accuracies and sample-based area estimates with confidence intervals at the 95% level from confusion matrices for all classes and both countries separately in two change maps (Table 3). For sample-based area estimation we used the stratified estimator from Olofsson et al. (2014). We acknowledge that, according to good practices for accuracy assessments and area estimation (sensu Olofsson et al., 2014), the reference data that was available to us was not ideal, because we had to visually interpret for most time steps the same imagery that was used to derive the map. This can potentially contribute to uncertainty in classification and subsequently, accurate change analysis, for example in cases, when a misclassified object is poorly distinguishable in the reference source.

2.6. Sensitivity analysis of the effects of the segmentation scale parameter on change detection accuracy for Corona and Landsat data

The selection of the scale parameter has a strong effect on image segmentation, which is why we conducted a sensitivity analysis to identify the optimal scale parameter, and to test how robust our approach is. For this sensitivity analysis, we used a subset of the Corona KH-4B mosaic and the Landsat 8 mosaic. Since Corona data has only one band, we averaged pixel values in Landsat's bands 2, 3, and 4, to match with the spectral range in Corona images (500–680 μm) as closely as possible.

We tested scale parameters of 10, 20, 50, 100, 150, 200, 250, and 300 for both Corona and Landsat data in eCognition, and held all other parameters constant. The “scale factor” is essentially a heterogeneity threshold in the image object delineation (Benz et al., 2004), which is why we calculated two measures of “goodness” to evaluate image objects: intra-segment homogeneity and inter-segment heterogeneity (Johnson and Xie, 2011). Ideally, image object should be highly homogenous and very different from each other, i.e., intra-segment homogeneity should be low and inter-segment heterogeneity should be high. Intra-segment homogeneity was measured by area-weighted variance in pixel values (Johnson and Xie, 2011), with lower variance indicating higher internal homogeneity. Inter-segment heterogeneity

Table 3
Error matrix for the forested area change maps from 1967 to 1989 (above) and 1989 to2015 (below). Accuracy measures are presented with a 95% confidence interval.

		Stable forest	Stable non-forest	Forest gain	Forest loss	Total	Users's accuracy	Producer's accuracy	Overall accuracy
Latvia 1967–1989		Reference							
Map	Stable forest	0.187	0.008	0.017	0.000	0.212	0.88 ± 0.13	0.88 ± 0.13	0.92 ± 0.05
	Stable non-forest	0.013	0.519	0.000	0.013	0.546	0.95 ± 0.07	0.95 ± 0.05	
	Forest gain	0.008	0.017	0.168	0.000	0.193	0.87 ± 0.14	0.91 ± 0.11	
	Forest loss	0.003	0.003	0.000	0.042	0.048	0.88 ± 0.17	0.76 ± 0.36	
	Total	0.212	0.548	0.185	0.056	1			
Russia 1967–1989		Reference							
Map	Stable forest	0.297	0.010	0.005	0.005	0.317	0.94 ± 0.06	0.94 ± 0.06	0.93 ± 0.04
	Stable non-forest	0.008	0.383	0.017	0.000	0.408	0.94 ± 0.07	0.94 ± 0.05	
	Forest gain	0.006	0.013	0.214	0.000	0.233	0.92 ± 0.09	0.91 ± 0.10	
	Forest loss	0.003	0.001	0.000	0.038	0.042	0.91 ± 0.09	0.89 ± 0.20	
	Total	0.315	0.406	0.236	0.043	1			
Latvia 1989–2015		Reference							
Map	Stable forest	0.268	0.015	0.015	0.015	0.312	0.86 ± 0.15	0.92 ± 0.09	0.91 ± 0.06
	Stable non-forest	0.012	0.493	0.000	0.012	0.518	0.95 ± 0.07	0.96 ± 0.06	
	Forest gain	0.004	0.004	0.069	0.000	0.076	0.90 ± 0.13	0.79 ± 0.27	
	Forest loss	0.006	0.003	0.003	0.080	0.093	0.86 ± 0.13	0.75 ± 0.26	
	Total	0.290	0.515	0.087	0.108	1			
Russia 1989–2015		Reference							
Map	Stable forest	0.459	0.014	0.000	0.007	0.480	0.96 ± 0.05	0.97 ± 0.03	0.93 ± 0.04
	Stable non-forest	0.008	0.331	0.015	0.008	0.362	0.92 ± 0.08	0.94 ± 0.06	
	Forest gain	0.002	0.007	0.077	0.002	0.088	0.88 ± 0.10	0.80 ± 0.18	
	Forest loss	0.002	0.002	0.004	0.061	0.070	0.87 ± 0.12	0.78 ± 0.21	
	Total	0.471	0.354	0.097	0.077	1			

was measured as the global Moran's I index values for each scale. Moran's I is an indicator of autocorrelation and measures the similarity of objects in relation to their neighbors (Espindola et al., 2006; Fotheringham et al., 2000). Positive Moran's I values indicate spatial clustering, whereas negative values indicate spatial dispersion (Goodchild, 1986), and lower values indicate high inter-segment heterogeneity. We based our calculations of Moran's I on the mean pixel values in every image object and the squared inverse distance when considering the spatial relationships among neighboring image objects.

Once the image objects were generated for each scale factor, we assigned forest and non-forest classes to image objects using the approach described above. After that we produced five change maps for 1967–2015 corresponding to scale parameter values of 10, 50, 100, 200 and 300 and performed accuracy assessments for each using a stratified random sampling with 50 stand-alone validation points, which we also visually interpreted (Table 6), which resulted in Overall, User's and Producer's accuracies, as well as confidence intervals (at the 95% level).

2.7. Propensity score matching

In addition to comparing forest cover changes for the total area in each country, we employed Propensity Score Matching (Butsic et al. 2017) to select focal cells for detailed analysis of forest pattern change, in order to account for differences in average environmental conditions and accessibility. First, we applied a 15 × 15 km square grid to divide the study area into 98 cells, and, second, we calculated the propensity score S_p for each cell. The score was calculated from three control variables for each cell: D_n – distance to the nearest town (km), E_m – mean elevation (m a.s.l.), and F_i – initial forest area proportion (%) in 1967 Eq. (1), as proxies for major potential drivers of land use change.

$$S_p = D_n \times E_m \times F_i \quad (1)$$

Last, we identified three pairs of matching cells in Latvia and Russia that had similar propensity scores to compare their changes in forest area and patterns in detail (Fig. 1). We selected the first cell from each pair in Latvia by randomly choosing from the list of cell IDs. The first pair was Balvi & Ladino (propensity scores 64,931,927 and 67,047,094, respectively), the second pair Rugaji & Kustovo (176,790,851 and 171,672,734) and the third Andrupene & Sergiye (365,799,507 and 372,284,570).

2.8. Morphological spatial pattern analysis

In order to describe changes of forest patterns and to calculate forest fragmentation in the entire study area and in each of the six focal cells we applied used Morphological Spatial Pattern Analysis (Soille and Vogt, 2009) in Guidos Toolbox 2.6 (Vogt and Riitters, 2017). Specifically, we calculated the metrics Core, Islet, Perforation, Edge, Loop, Bridge and Branch as indicators of spatial pattern of forest cover for each of our three dates. These metrics capture the proportions of the area of each category of forest cover pattern relative to the total forested area. The Core metric quantifies the proportion of forest that is more than 60 m away from the forest perimeter, denoting forested areas with undisturbed conditions. The Islet metric captures the proportion of forest that occurs in small patches without core area, i.e., in structurally isolated patches of forest. The Perforation metric denotes the area of forest that is within 60 m of perimeter of a hole in forest, thus reflecting forest disturbance. The Edge metric is the proportion of forest within 60 m of the outside edge of forests, and those forests are typically influenced by neighboring habitats. Lastly, there are three metrics that reflect forest connectivity. The Loop metric is proportion of forest that is in corridors that connect to the same core area, the Bridge metric reflects the proportion of forest that connects two different core areas, and the Branch metric is the proportion of forest cover of dead-end connections to any forest cover objects. We applied a 8-neighbor rule and set the edge depth parameter for MSPA to 60 m (2 pixels), a conservative estimate of the depth of edge influence in hemiboreal forest (Moen and Jonsson, 2003; Tinker et al., 1998).

3. Results

3.1. The accuracy of forest cover mapping

We produced two pairs of change maps for Latvia and Russia, one

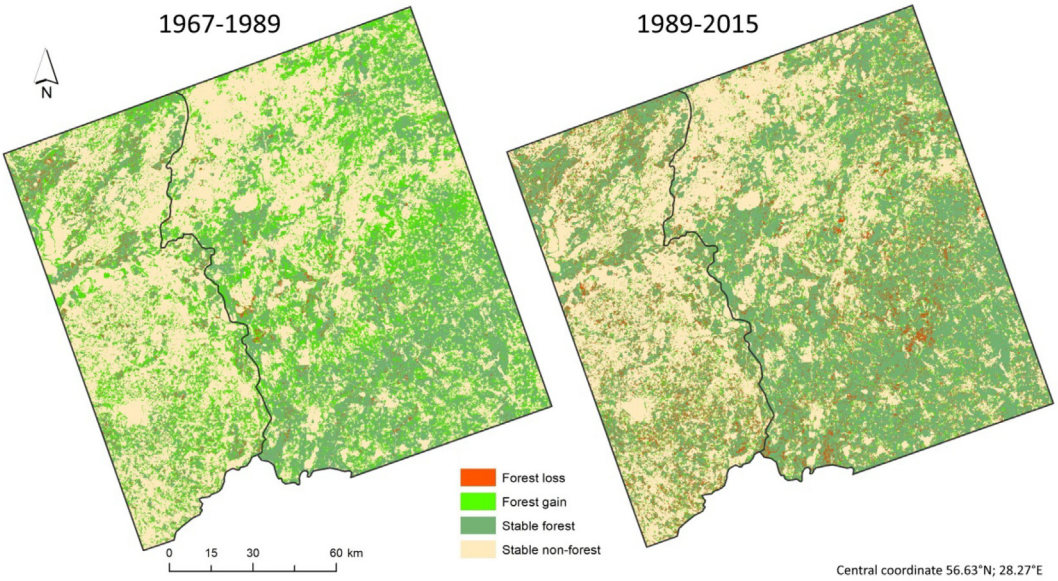

Fig. 3. Change maps of study area for periods of 1967–1989 and 1989–2015.

for 1967–1989 and one for 1989–2015 (Fig. 3), and all four had high levels of accuracy (Table 3). For the 1976–1989 change maps, the overall accuracy was 92% for Latvia and 93% for Russia. In Latvia user's accuracies for the change map classes ranged from 88 to 95%, and producer's accuracies from 76 to 95%. In Russia user's accuracy reached 91–94% and producer's accuracy was from 89 to 94%. Stable non-forest class had the lowest commission errors in both countries, with only 2.5–2.6% of the study area classified incorrectly. Forest loss class in Latvia had the lowest user's accuracy (76%) due to higher commission errors, when stable non-forest and stable forest areas were classified as forest loss (these errors occurred on 0.6% of our study area). Forest gain and forest loss classes in Russian part of study area had higher accuracy compared to Latvian part with commission errors of 0.4% to 1.9% (respectively) of the study area.

For 1989–2015 the overall accuracy was also high (91% in Latvia and 93% in Russia). User's accuracies were similar between countries, ranging from 86 to 95% in Latvia, and from 87 to 96% in Russia. Producer's accuracies ranged from 75 to 96% in Latvia and from 78 to 97% in Russia (Table 3). Stable land cover classes had higher user's accuracies in both countries (92–95% for stable non-forest, and 92% for stable forest in Russia) than the change classes (86%–90% in Latvia and 87–88% in Russia), with the exception of stable forest class in Latvia (86%). Relatively low commission errors for stable forest in Russia resulted in 2.4% of the study area being misclassified as stable forest even though it was in fact stable non-forest or forest loss. The forest loss class had a relatively high omission error, in that 1.7% of actual Forest loss area was misclassified as other classes.

3.2. General changes in forest cover and forest patterns

Sample-based forest area differed considerably between the two countries, and between the two periods. During 1967–1989, stable forest area was 21.2% (± 8.4 pp) in Latvia and 31.5% (± 7.5 pp) in Russia (95% confidence level) (Table 4). The majority of the forest area increase took place during this period when forest gain reached impressive 18.5% (± 7.8 pp) in Latvia and 23.6% (± 7.5 pp) in Russia. Forest loss was only 5.6% (± 3.5 pp) in Latvia and 4.3% (± 1.5 pp) in Russia. The rate of forest gain for 1967–1989 was 0.84% per year in Latvia and 1.1% per year in Russia.

During the 1989–2015 period, forest gain proportion decreased considerably, to just 8.7% (± 4.4 pp) in Latvia and 9.7% (± 3.4 pp) in Russia. However, during this period forest loss almost balanced forest gain and reached 10.8% (± 5 pp) in Latvia and 7.7% (± 3.1 pp) in Russia.

Table 4
Sample-based area estimates for the change map classes for Latvia and Russia.

	Area (1000 ha)	Proportion (%)	Area (1000 ha)	Proportion (%)
	Latvia 1967–1989		Russia 1967–1989	
Stable forest	165.5	21.2%	452.3	31.5%
Stable non-forest	428.1	54.8%	583.5	40.6%
Forest gain	144.7	18.5%	338.5	23.6%
Forest loss	43.5	5.6%	62.0	4.3%
	Latvia 1989–2015		Russia 1989–2015	
Stable forest	227.1	29.0%	677.2	47.1%
Stable non-forest	403.0	51.5%	508.9	35.4%
Forest gain	67.8	8.7%	139.2	9.7%
Forest loss	84.2	10.8%	111.0	7.7%

From 1989 to 2015, stable forest proportion increased in both countries (Table 4, Fig. 5), reaching 29% (± 12.4 pp) in Latvia and 47.1% (± 10 pp) in Russia. Consequently, stable non-forest area shrunk during 1989–2015 compared to 1967–1989 to 51.5% (± 13.7 pp) in Latvia and 35.4% (± 9.5 pp) in Russia.

Our forest pattern analysis showed that concomitant to the general increase in forest cover there was a decrease in forest fragmentation. For example, from 1967 to 1989 forest core areas increased by 131% in Latvia and 134.5% in Russia (Table 5). The rapid increase in forested areas from 1967 to 1989 contributed the most to the overall increase in core forest area, while 1989–2015 core forest area unexpectedly declined (Fig. 6). Edge area increased in Latvia (by 28.3%) but slightly decreased in Russia (by 5%). The proportion of islet (isolated forest patch) area decreased considerably from 1967 to 1989 (−23.2% in Latvia and − 34.2% in Russia) but increased from 1989 to 2015 (by 252% and 5.2%, respectively). Overall, the increase of forest cover resulted in a strong increase of core forest areas and hence a de-fragmentation of forest cover.

3.3. Forest pattern change in focal cells

Comparisons of forest changes of the fully study area on both sides of the border are confounded by the fact that Latvia and Russia differ

Table 5
Changes in spatial pattern metric values for forest cover during 1967–1989 and 1989–2015.

	Latvia		Russia	
Spatial pattern class	1967–1989	1989–2015	1967–1989	1989–2015
Core	131.0%	−56.8%	134.5%	−4.0%
Islet	−23.2%	252.0%	−34.2%	5.2%
Edge	28.3%	23.6%	−5.0%	18.7%
Perforation	114.2%	−77.1%	185.8%	14.8%
Bridge	−46.6%	293.5%	−65.3%	18.2%
Branch	16.4%	65.4%	−3.4%	31.5%
Loop	−34.6%	106.7%	−20.5%	−15.2%

MSPA metrics: Core – the area proportion of forest cover objects excluding 60 m buffer; Islet – area proportion of forest cover patches without Core area; Perforation – area proportion of 60 m buffers along the perimeter of a hole in forest cover; Edge – area proportion of forest cover inside 60 m buffers of all objects; Loop – area proportion of forest cover connections to the same Core area; Bridge - area proportion of forest cover connections to the different Core area; Branch – area proportion of dead-end connections to any forest cover objects.

somewhat in terms of elevation, distance to the nearest city, and initial forest cover. That is why we also made comparisons for our focal cells, where we controlled for those differences (Fig. 4). The trends in our focal cells generally confirmed our study-area wide comparison, and our forest pattern metrics indicated similar trends in all three pairs of focal cells (Fig. 6). Forest spatial pattern was more similar for cells within the same countries than for matching cells across the border. For instance, core forest area increased in all focal areas before 1989, but after 1989 core forest area decreased only in those in Latvia. Sergiye and Ladino areas (both in Russia) had the most rapid increase in core forest areas (Fig. 6), and the increase in core forest areas was more rapid on the Russian side, mirroring the overall forest area increase. Areas of both islets (patches) and landscape bridges (corridors) declined from 1967 to 1989 but remained largely unchanged thereafter.

We found the biggest differences between Andrupene (Latvia) and Sergiye (Russia) cells. Rapid increase in core area in Sergiye from 1967 to 1989 was the most striking difference: during this period core forest area increased by 118.6% and continued to grow thereafter by 6.7%. Meanwhile in Andrupene core forest area increased by 151% from 1967 to 1989, but declined by −36.1% thereafter. Rugaji (Latvia) and Kustovo (Russia) were the most similar pair in terms of trends and magnitudes of change in functional landscape elements. Again, the main difference occurred after 1989, when core forest area continued to increase in Kustovo (+19.2%), while experiencing a notable decrease in Rugaji (−41.3%). The growth of core forest area and the decrease of islet area in almost all focal cells from 1967 to 2015 showed that the expansion of forest cover resulted consistently in the defragmentation of forest cover.

3.4. Analysis of change detection errors for Corona and Landsat data

Our sensitivity analysis of the effects of the scale parameter for the object-based image analysis found that the segmentation was quite sensitive to the scale parameters, but the change analyses were not, and similar scale parameters were ideal for both Corona and Landsat data. In general, a higher scale parameter results in higher intra-segment heterogeneity, and lower inter-segment heterogeneity, as would be

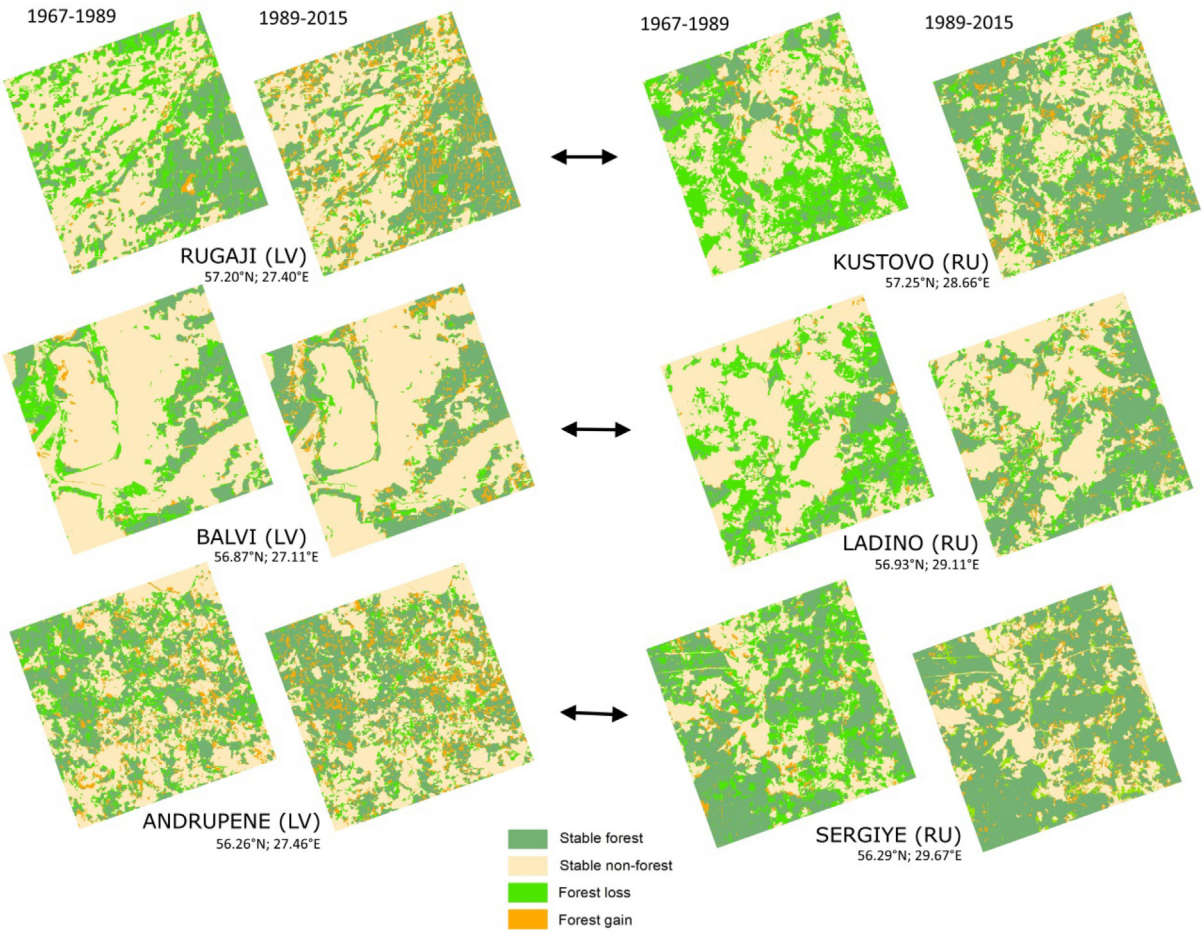

Fig. 4. Change maps of six focal areas for periods of 1967–1989 and 1989–2015.

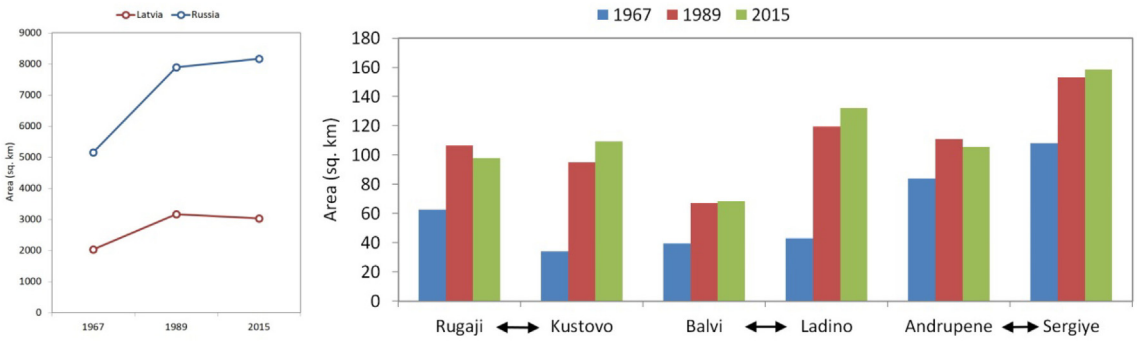

Fig. 5. Forested area dynamics in entire study area (left) and focal areas (right).

expected (Fig. 7). The optimal balance of relatively high intra-segment homogeneity (low weighted spectral variance) and relatively high inter-segment heterogeneity (low Moran's I value), occurred for Corona at a scale parameter of 50 and for Landsat at 100, but a scale parameter of 100 was also quite good for Corona. Ultimately though, the question is how sensitive our change analyses were to the scale parameter.

To measure the effects of the scale parameters, we estimated the accuracy of resulting forest change maps for scale factors 10, 50, 100, 200, and 300 (Table 6). We attained the highest overall accuracy using scale factors of 50 and 100 (90% and 92%, respectively). Scale-100 maps had user's accuracies ranging from 83% to 92%, with the highest commission errors for forest gain and loss classes. Producer's accuracy reached 95% for stable non-forest and forest gain classes. Second-best overall accuracy was for the scale-50 maps with an overall accuracy of 90% and similar levels of commission and omission errors, except for stable forest class with 15% omission error. Scale-300 maps had the lowest overall accuracy of 82%, their stable forest and stable non-forest classes had commission errors of 15–23%, while the forest gain and forest loss classes had high accuracy with only 8% commission error. These maps also had the highest omission error of 57% for forest loss class. For the scale-10 maps the overall accuracy was 86% and there were high commission errors for stable forest and stable non-forest classes (15%) and for forest loss class (17%). Forest loss class had very high omission error (51%).

In summary, the scale parameter had strong effects on the image segmentation, but our forest change analyses were less affected, as indicated by the fact that classification accuracy was high for a large range of scale parameters. Furthermore, calculating intra- and inter-segment heterogeneity for a range of scale parameters can quickly identify the optimal scale parameter, which was 100 for our data.

4. Discussion

4.1. Cross-border comparison of forest cover change

Our study showed that the majority of the forest cover increase in the Latvian-Russian border area occurred already during Soviet rule, i.e., from 1967 to 1989, which surprised us. During this time the afforestation rate was much higher than from 1989 to 2015, i.e., the time of the post-Soviet transition. The beginning of our study period coincided with the beginning of new Soviet agricultural policy, which started in 1965 when capital investments in agriculture increased greatly (Boruks, 2003; Lerman et al., 2004). In 1950 many of smaller kolkhozes in Latvia were merged in an effort to increase their productivity (Boruks, 2003), which led to the shift of economic centers to larger rural settlements and the abandonment of smaller ones. This was accompanied by depopulation in certain areas (Melluma, 1994). Several phases of kolkhoz unification followed in subsequent decades. Intensified cultivation focused mostly on lands that were drained and readily accessible by roads, in turn causing the abandonment of more remote lands that were previously cultivated by individual private farms before land nationalization in 1940 (Boruks, 2003). From 1967 to 1989 we found higher rates of Forest gain in Russia (1% annually) than in Latvia (0.78% annually). Likely reasons are that population density in Latvia was double that in Russia, and that in Latvia land use legacies of intensive cultivation persisted throughout Soviet time.

The majority of the overall forest cover increase occurred in Russia, which surprised us because forest cover in 1967 was already higher there (32.5%) than in Latvia (20.7%). A reason for the higher initial forest cover may be that the collectivization of agricultural production and merging of cultivated lands occurred two decades earlier in Russia than in Latvia (Ioffe et al., 2006; Ioffe and Nefedova, 2004), and that meant that the marginalization of the most remote lands probably happened already before WW II. Another reason for more widespread forest cover increase after 1967 may have been the displacement of population due to war, and repressions, and that hardships of rural life decreased the number of people working in the agricultural sector caused the depopulation of the already sparsely populated region before 1989 (Solanko and Tekoniemi, 1999), plus the decrease in government subsidies for farming during the 1990s (Prishchepov et al., 2013). Both sections of the study area depopulated considerably during the timespan of our study, but while in Latvian section the number of inhabitants decreased by 32.6% (1979–2015), it declined in the Russian section by 46.3% (1970–2015). These rates of population declines are among the highest in European Russia (Central Bureau of Statistics, n.d.; Ioffe et al., 2006; ROSSTAT 2015; Vsesojuznaya Perepis' Naseleniya, 1970). The lack of human capital and low productivity soils are major reasons of land abandonment for the border regions of Russia (Kolosov et al., 2017). We suggest that both population and policy factors were important factors, which interactively caused agricultural land abandonment.

During the post-socialist era, we found that land use change rates were lower and quite similar in both countries. This surprised us, given that Latvia has been part of the EU since 2004. However, abandonment of agricultural lands was high in both countries during the 1990s, when cultivated area declined by 39% in Russia and 38% in Latvia (Prishchepov et al., 2012), even though there were quite different land policies in both countries. Wide-scale land restitution and rapid land reforms in Latvia during 1990s created large number of small private land and forest owners, half of all forests remained property of the state. In contrast, land holdings that were privatized in Russia were limited in size and all forests remained in the ownership of the state (Lerman et al., 2004). However, land abandonment after 1989 may not have resulted in large forest area increase yet because succession and natural afforestation of abandoned farmlands in hemiboreal Europe happens relatively slowly (Ruskule et al., 2016), and further increases in forest area may occur in the future.

Latvia's accession to the European Union in 2004 may have helped to slow the rate of agricultural abandonment, even though EU subsidies had limited effect in maintaining rural landscapes (Nikodemus et al., 2010), especially in more remote, hilly areas of the country. However, subsidies were important for agriculture in flat, fertile areas, which

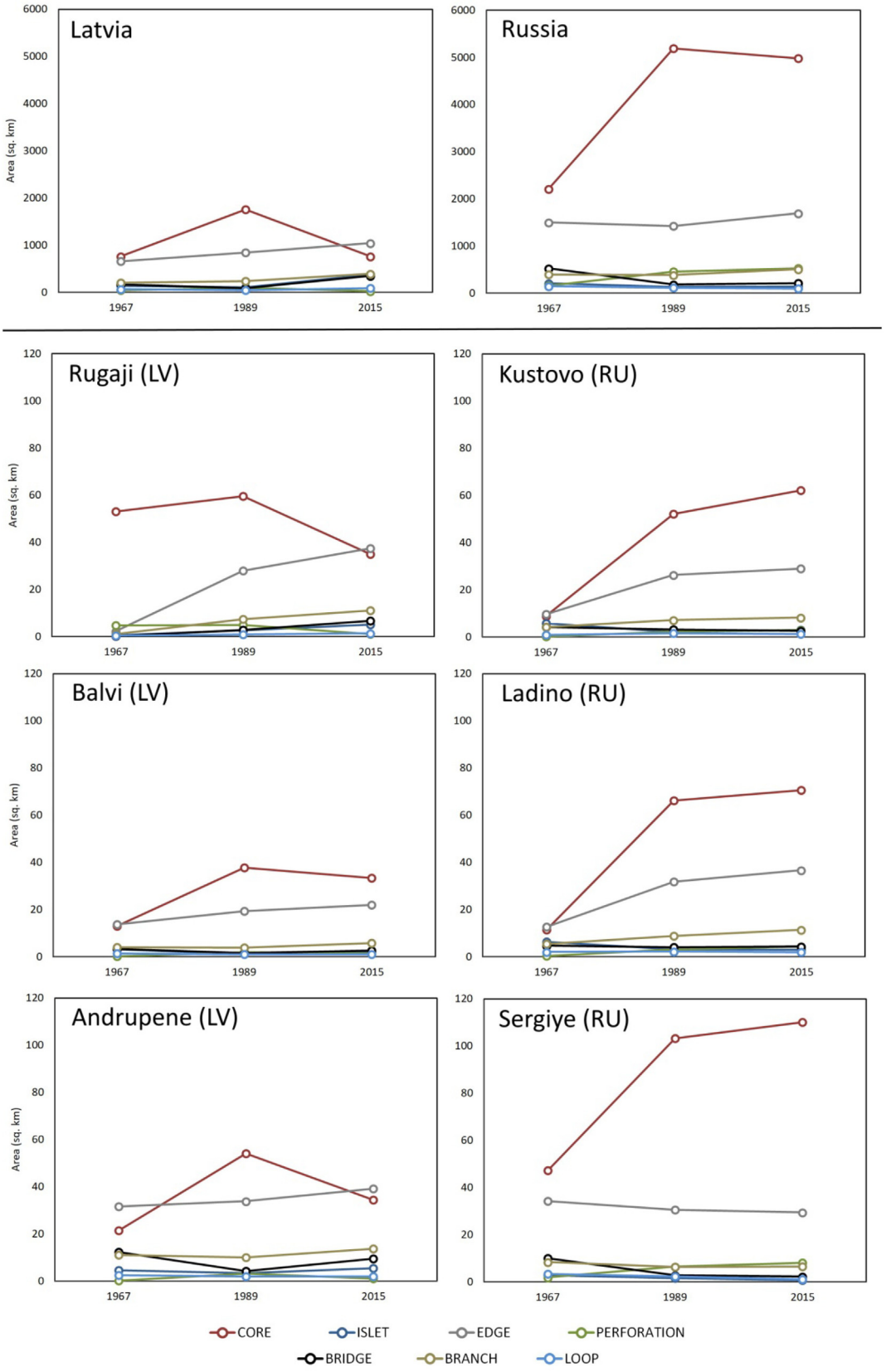

Fig. 6. Changes in forest cover pattern metrics in Latvian and Russian parts of study area (upper part) and in selected focal cells (lower part) between 1967 and 2015.

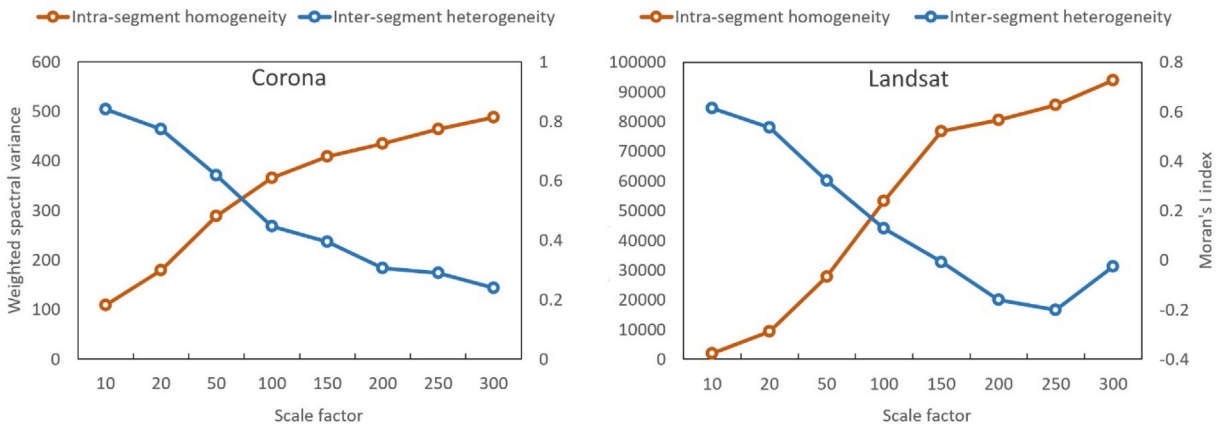

Fig. 7. Sensitivity analysis of object-based image analysis scale factor on the accuracy of object delineation measured by area-weighted variance and global Moran's I index.

were intensively cultivated during the Soviet time, and there the new subsides slowed forest regrowth (Vanwambeke et al., 2012). However, the EU also provided subsidies to support the conversion of unused farmland to forest, and Latvia's Forest policy supports afforestation of abandoned lands (Cabinet of Ministers, 1998).

Two other studies in Latvia, roughly covering our study period of 1989–2015, reported much higher rates of agricultural abandonment (Vanwambeke et al., 2012) and afforestation (Fonji and Taff, 2014) but for other regions of Latvia. This demonstrates the spatial variability of forest area increase even in a relatively small country. Interestingly, the area of forest loss after 1989 in our study areas was larger than that of forest gain, mainly due to intensified logging, and infrastructure development. For example, multiple highways were built in Russia at that time causing some forest cover loss. Similarly, logging was more widespread in Latvian section of study area, accounting for the majority of 7.9% net forest loss. Since 2000 logging and forest management in Latvia have intensified (Rendenieks et al., 2015). Indeed, according to an analysis of annual Landsat satellite data since 2000 (Hansen et al., 2013), logging rates were five times higher in Latvia compared to Russia. A study by Potapov et al. (2015) mapped forest cover change in Eastern Europe for 1985–2012. They found an area of stable forest area that was larger (38.7% in Latvian section and 55.8% in Russian section) to what we found for 1989–2015 (31.9% and 47.3%, respectively). Furthermore, they reported less forest gain and more forest loss than we found. For example, until 1989 the forest loss area proportion was identical in Latvia and Russia (0.4%) in the dataset by Potapov et al. (2015), but after 1989 it was double in Latvia compared to Russia (3.2% vs. 1.4%). However, because the timespan of their analysis does not match ours exactly, some of these differences, especially in the case of forest gain, may be due to the temporal mismatch. Furthermore, it is important to note that change in the spatial pattern of forests alone is not a direct measure of forest loss. For example, deforestation can manifest itself in a range of MSPA metrics depending on the spatial distribution of clearcuts. This means that spatial pattern metrics must be interpreted in the context of estimated changes in forest area.

Our forest pattern analysis showed de-fragmentation on both sides of the border, but especially in Russia, resulting in the expansion of forest core area (MSPA's Core metric) and decrease of forest corridors (Bridge metric). Edge area increased, in conjunction with far fewer forest “islets”, because forests regrew mostly adjacent to existing forest tracts, thus contributing to the overall de-fragmentation of forest cover. This confirmed prior research in Latvia, which showed that linear and continuous afforestation from the forest edge results in more uniform stands and faster canopy closure compared to mosaic-type afforestation

Table 6
Accuracies of the forested area change maps from 1967 to 2015 for different segmentation scale factors. Accuracy measures are presented with a 95% confidence interval.

	Stable Forest	Stable Non-forest	Forest gain	Forest loss	
Scale 10					
Overall accuracy					0.86 ± 0.12
User's accuracy	0.85 ± 0.20	0.85 ± 0.20	0.92 ± 0.16	0.83 ± 0.22	
Producer's accuracy	0.74 ± 0.28	0.96 ± 0.20	0.92 ± 0.15	0.49 ± 0.49	
Scale 50					
Overall accuracy					0.90 ± 0.10
User's accuracy	0.85 ± 0.20	0.92 ± 0.15	0.92 ± 0.16	0.83 ± 0.22	
Producer's accuracy	0.74 ± 0.28	0.96 ± 0.06	1	0.71 ± 0.41	
Scale 100					
Overall accuracy					0.92 ± 0.05
User's accuracy	0.91 ± 0.12	0.95 ± 0.07	0.87 ± 0.14	0.88 ± 0.17	
Producer's accuracy	0.87 ± 0.13	0.95 ± 0.05	0.95 ± 0.10	0.76 ± 0.36	
Scale 200					
Overall accuracy					0.87 ± 0.12
User's accuracy	0.92 ± 0.15	0.85 ± 0.20	0.85 ± 0.20	0.92 ± 0.16	
Producer's accuracy	0.76 ± 0.26	0.97 ± 0.07	0.80 ± 0.32	0.75 ± 0.37	
Scale 300					
Overall accuracy					0.82 ± 0.14
User's accuracy	0.85 ± 0.20	0.77 ± 0.24	0.92 ± 0.16	0.92 ± 0.16	
Producer's accuracy	0.68 ± 0.29	0.95 ± 0.07	0.92 ± 0.15	0.43 ± 0.38	

(Ruskule et al., 2012). Because the majority of study area's forests are managed, the increase in the Perforation metric is mainly explained by intensified logging, as well as some infrastructure development and natural disturbances.

The forest area increase, and the defragementation of forest cover is likely positive for forest biodiversity, but there is also controversy in Latvia about the afforestation of abandoned croplands and grasslands, because afforestation reduces farmland biodiversity, and aesthetic value of landscapes when semi-natural grasslands vanish and forested patches merge (Bremer and Farley, 2010). For land managers, ongoing natural afforestation of abandoned agricultural lands generally presents three choices: intensification, extensification, or afforestation of these lands. Despite lower financial gains, local residents generally prefer natural afforestation over plantations, which could yield higher quality timber (Ruskule et al., 2013). However, because the availability of capital, subsidies, and willingness to maintain normative land use is limited in our study area, there are few options for rural landowners and government agencies.

4.2. Combining Corona and Landsat data for forest change mapping

We tested here the use of object-based image analysis for forest change analyses that utilize both Corona and Landsat data. Combining these two types of data is non-trivial given the strong differences in image characteristics such as spatial resolution, spectral detail, and number of bands. That raised the question which scale factor would be best for each type of data given that the scale factor directly influences the count, size and shape of resulting image objects (Darwish et al., 2003). Interestingly, we found that fairly similar scale factors were optimal for Corona and Landsat data (50 and 100, respectively). A scale factor of 100 for both datasets resulted in the highest overall accuracy of the forest change maps (92%). However, a scale factor of 50 was also very good (accuracy of 90%), and even for a scale factor of 200, the change maps were quite accurate (87%). These results suggest that when analyzing forest changes from Corona and Landsat data, object based image analyses are fairly robust in terms of the scale parameter, but we nevertheless recommend to select the optimal scale parameter based on an analyses of inter- and intra-segment heterogeneity, as we demonstrate in our results.

To the best of our knowledge, our study was the first to utilize object-based image analysis to assess forest change from Corona and Landsat data. As such, our approach differed from prior studies of change that were pixel-based or employed image texture in moving windows to identify land cover classes (Shahtahmassebi et al. 2017; Song et al., 2015). Those studies resulted also in high classification accuracies, and it would be interesting to compare approaches, but that was beyond the scope of our study. Originally, Corona images were only visually interpreted, often by leveraging its stereoscopical abilities. Our approach, which uses automated feature recognition from Corona images and camera alignment reconstruction for the image rectification, enables fast and efficient land use change analyses over broad areas. Object-based image analysis worked well, is generally advantageous for panchromatic imagery, and our results suggest that it is a promising approach for long-term change analyses that integrate Corona and Landsat data.

5. Conclusions

Land use and land cover change studies rarely use Corona images for large-area mapping (Song et al., 2015; Tappan et al., 2000). Our results demonstrated that these historical, pre-digital era satellite images can be successfully used for land cover classifications and change detection of large areas. Harnessing the stereo capabilities of Corona imagery with Structure-from-Motion photogrammetry (Ullman, 1979), in conjunction with object-based image analysis, allowed us to extend the timeline of our analysis by almost twenty years prior to the advent of 30-m Landsat data. The workflow by (Nita et al., 2018), which we used for the orthorectification of the Corona images, was efficient in terms of time and computational power and resulted in orthomosaics with high geolocational accuracy. Our object-based approach was well-suited for analyzing Corona images, which have a considerable amount of noise and scanning errors (Gheyle et al., 2011), and also was robust to the internal spectral heterogeneity of forested areas.

For land use science it is important to devise a robust and efficient methodology to integrate pre-Landsat imagery with the Landsat archive to expand the length of time series that document and analyze land cover and land use change and forest disturbance mapping (sensu. Huang et al., 2009). Given that our study produced surprising results, most notably widespread agricultural abandonment prior to the collapse of the Soviet Union, we suggest that long-term analyses of forest area change, and of other land cover types, can benefit greatly from Corona imagery.

Declaration of Competing Interest

None.

Acknowledgements

We are grateful to the Baltic-American Freedom Foundation for funding this research and the University of Wisconsin-Madison for support in research. This work was financially supported by the specific support objective activity 1.1.1.2. “Post-doctoral Research Aid” (Project Id. 1.1.1.2/16/I/001) of the Republic of Latvia, funded by the European Regional Development Fund, to postdoc Z. Rendenieks research project No. 1.1.1.2/VIAA/2/18/277 “The role of new woodlands in the change of spatial structure of Latvian landscapes from 1967 to 2017”, University of Latvia grant No. AAp2016/B041//Zd2016/AZ03 within the project “Climate change and sustainable use of natural resources” (to O. Nikodemus), and by NASA's Land Cover and Land Use Change Program. We thank two anonymous reviewers for their constructive and valuable comments.

Declaration of Competing Interest

The authors declare that they have no known competing financial interests or personal relationships that could have appeared to influence the work reported in this paper.

References

Vsesojuznaya Perepis” Naseleniya, 1970. Vsesojuznaya Perepis' Naseleniya. http://demoscope.ru/weekly/ssp/rus70_reg1.php.

ROSSTAT, 2015. Chislennost’ Naselyeniya Rossiyskoy Federacii’. http://www.gks.ru/free_doc/doc_2015/bul_dr/mun_obr2015.rar accessed 8.11.18.

Munteanu, C., Kuemmerle, T., Boltiziar, M., Lieskovsky, J., Mojses, M., Kaim, D., Konkoly-Gyuró, É., Mackovčin, P., Mueller, D., Ostapowicz, K., et al., 2017. Nineteenth-century land-use legacies affect contemporary land abandonment in the Carpathians. Reg. Environ. Chang. 17, 2209–2222. https://doi.org/10.1007/s10113-016-1097-x.

Angelstam, P., Dönz-Breuss, M., 2004. Measuring forest biodiversity at the stand scale: an evaluation of indicators in European forest history gradients. Ecol. Bull. 305–332. https://doi.org/10.2307/20113319.

Bartha, S., Meiners, S.J., Pickett, S.T.A., Cadenasso, M.L., 2003. Plant colonization windows in a Mesic old field succession. Appl. Veg. Sci. 6, 205–212. https://doi.org/10.1111/j.1654-109X.2003.tb00581.x.

Bell, S., Montarzino, A., Aspinall, P., Penēze, Z., Nikodemus, O., 2009. Rural society, social inclusion and landscape change in central and Eastern Europe: a case study of Latvia. Sociol. Rural. 49, 295–326. https://doi.org/10.1111/j.1467-9523.2009.00480.x.

Benz, U.C., Hofmann, P., Willhauck, G., Lingenfelder, I., Heynen, M., 2004. Multi-resolution, object-oriented fuzzy analysis of remote sensing data for GIS-ready information. ISPRS J. Photogramm. Remote Sens. 58, 239–258.

Blaschke, T., 2010. Object based image analysis for remote sensing. ISPRS J. Photogramm. Remote Sens. 65, 2–16.

Bolch, T., Buchroithner, M., Pieczonka, T., Kunert, A., 2008. Planimetric and volumetric glacier changes in the Khumbu Himal, Nepal, since 1962 using Corona, Landsat TM

and ASTER data. J. Glaciol. 54, 592–600.
Boruks, A., 2003. Zeme, Zemnieks Un Zemkopība Latvijā. No Senākiem Laikiem līdz Mūsdienām. Latvijas Lauksaimniecības Universitāte, Jelgava.
Bremer, L.L., Farley, K.A., 2010. Does plantation forestry restore biodiversity or create green deserts? A synthesis of the effects of land-use transitions on plant species richness. Biodivers. Conserv. 19, 3893–3915. https://doi.org/10.1007/s10531-010-9936-4.
Butsic, V., Lewis, D.J., Radeloff, V.C., Baumann, M., Kuemmerle, T., 2017. Quasi-experimental methods enable stronger inferences from observational data in ecology. Basic Appl. Ecol. 19, 1–10. https://doi.org/10.1016/j.baae.2017.01.005.
Cabinet of Ministers, 1998. Latvian Forest Policy. Parliament of Latvia.
Cabinet of Ministers, 2006. Ministru kabineta noteikumi Nr. 903. Parliament of Latvia.
Central Bureau of Statistics, 2018. Population number and change. https://www.csb.gov.lv/en/statistics/statistics-by-theme/population/number-and-change.
Chabak, E., 2011. Lesa dostupny, no izpolzuyutsa slabo. LesPromInform 6, 54–56.
Darwish, A., Leukert, K., Reinhardt, W., 2003. Image segmentation for the purpose of object-based classification. In: IGARSS 2003. 2003 IEEE International Geoscience and Remote Sensing Symposium. Proceedings (IEEE Cat. No. 03CH37477), pp. 2039–2041.
Dashora, A., Lohani, B., Malik, J.N., 2007. A repository of earth resource information – CORONA satellite programme. Curr. Sci. 92, 926–932. https://doi.org/10.2307/24097673.
Espindola, G.M., Câmara, G., Reis, I.A., Bins, L.S., Monteiro, A.M., 2006. Parameter selection for region-growing image segmentation algorithms using spatial autocorrelation. Int. J. Remote Sens. 27, 3035–3040.
Fonji, S., Taff, G.N., 2014. Using satellite data to monitor land-use land-cover change in North-Eastern Latvia. Springerplus 3, 61. https://doi.org/10.1186/2193-1801-3-61.
Fotheringham, A.S., Brunsdon, C., Charlton, M., 2000. Quantitative Geography: Perspectives on Spatial Data Analysis. Sage.
Galiatsatos, N., 2009. The shift from film to digital product: focus on CORONA imagery. Photogrammetrie-Fernerkundung-Geoinformation 2009, 251–260.
Galiatsatos, N., Donoghue, D.N.M., Philip, G., 2007. High resolution elevation data derived from stereoscopic CORONA imagery with minimal ground control. Photogramm. Eng. Remote Sens. 73, 1093–1106.
Gheyle, W., Bourgeois, J., Goossens, R., Jacobsen, K., 2011. Scan problems in digital CORONA satellite images from USGS archives. Photogramm. Eng. Remote Sens. 77, 1257–1264. https://doi.org/10.14358/PERS.77.12.1257.
Goodchild, M.F., 1986. Spatial Autocorrelation. CATMOG, 47, Norwich.
Goossens, R., De Wulf, A., Bourgeois, J., Gheyle, W., Willems, T., 2006. Satellite imagery and archaeology: the example of CORONA in the Altai Mountains. J. Archaeol. Sci. 33, 745–755.
Grīne, I., 2009. Lauku iedzīvotāju un apdzīvojuma telpiskās struktūras izmaiņas pēc Otrā pasaules kara (Cēsu rajona teritorijas). Doctoral dissertation. University of Latvia, Riga.
Gurjar, S.K., Tare, V., 2019. Estimating long-term LULC changes in an agriculture-dominated basin using CORONA (1970) and LISS IV (2013–14) satellite images: a case study of Ramganga River, India. Environ. Monit. Assess. 191, 217.
Gutman, G., Radeloff, V.C., 2017. Land-Cover and Land-Use Changes in Eastern Europe after the Collapse of the Soviet Union in 1991. https://doi.org/10.1007/978-3-319-42638-9.
Hansen, M.C., Potapov, P.V., Moore, R., Hancher, M., Turubanova, S.A., Tyukavina, A., Thau, D., Stehman, S.V., Goetz, S.J., Loveland, T.R., Kommareddy, A., Egorov, A., Chini, L., Justice, C.O., Townshend, J.R.G., 2013. High-resolution global maps of 21st-century Forest cover change. Science 342, 850–853. https://doi.org/10.1126/science.1244693.
Hossain, M.D., Chen, D., 2019. Segmentation for object-based image analysis (obia): a review of algorithms and challenges from remote sensing perspective. ISPRS J. Photogramm. Remote Sens. 150, 115–134.
Huang, C., Goward, S.N., Schleeweis, K., Thomas, N., Masek, J.G., Zhu, Z., 2009. Dynamics of national forests assessed using the Landsat record: case studies in eastern United States. Remote Sens. Environ. 113, 1430–1442. https://doi.org/10.1016/j.rse.2008.06.016.
Ioffe, G., Nefedova, T., 2004. Marginal farmland in European Russia. Eurasian Geogr. Econ. 45, 45–59. https://doi.org/10.2747/1538-7216.45.1.45.
Ioffe, G., Nefedova, T., Zaslavsky, I., 2004. From spatial continuity to fragmentation: the case of Russian farming. Ann. Assoc. Am. Geogr. 94, 913–943. https://doi.org/10.1111/j.1467-8306.2004.00441.x.
Ioffe, G., Nefedova, T., Zaslavsky, I., 2006. The End of Peasantry? The Disintegration of Rural Russia. University of Pittsburgh Press, Pittsburgh.
Ioffe, G., Nefedova, T., de Beurs, K., 2012. Land abandonment in Russia. Eurasian Geogr. Econ. 53, 527–549. https://doi.org/10.2747/1539-7216.53.4.527.
Johnson, B., Xie, Z., 2011. Unsupervised image segmentation evaluation and refinement using a multi-scale approach. ISPRS J. Photogramm. Remote Sens. 66, 473–483. https://doi.org/10.1016/J.ISPRSJPRS.2011.02.006.
Jones, A., Montanarella, L., Jones, R., 2005. Soil Atlas of Europe. European Commission, Luxembourg.
Kolosov, V., Medvedev, A., Zotova, M., 2017. Comparing the development of border regions with the use of GIS (the case of Russia). Geogr. Pol. 90, 47–61. https://doi.org/10.7163/GPol.0090.
Kuemmerle, T., Kaplan, J.O., Prishchepov, A.V., Rylsky, I., Chaskovskyy, O., Tikunov, V.S., Müller, D., 2015. Forest transitions in Eastern Europe and their effects on carbon budgets. Glob. Chang. Biol. 21 (8), 3049–3061.
Kuemmerle, T., Olofsson, P., Chaskovskyy, O., Baumann, M., Ostapowicz, K., Woodcock, C.E., Houghton, R.A., Hostert, P., Keeton, W.S., Radeloff, V.C., 2011. Post-soviet farmland abandonment, forest recovery, and carbon sequestration in western Ukraine. Glob. Chang. Biol. 17, 1335–1349. https://doi.org/10.1111/j.1365-2486.2010.02333.x.
Kuemmerle, T., Levers, C., Erb, K., Estel, S., Jepsen, M.R., Müller, D., Plutzar, C., Stürck, J., Verkerk, P.J., Verburg, P.H., Reenberg, A., 2016. Hotspots of land use change in Europe. Environ. Res. Lett. 11, 64020. https://doi.org/10.1088/1748-9326/11/6/064020.
Lauer, D.T., Morain, S.A., Salomonson, V.V., 1997. The Landsat program: its origins, evolution, and impacts. Photogramm. Eng. Remote Sens. 63, 831–838.
Lerman, Z., Csaki, C., Feder, G., 2004. Agriculture in Transition: Land Policies and Evolving Farm Structures in Post-Soviet Countries. Lexington books, New York.
Lorenz, H., 2004. Integration of Corona and Landsat thematic mapper data for bedrock geological studies in the high Arctic. Int. J. Remote Sens. 25, 5143–5162.
Mathijs, E., Swinnen, J.F.M., 1998. The economics of agricultural decollectivization in east Central Europe and the former Soviet Union. Econ. Dev. Cult. Chang. 47, 1–26. https://doi.org/10.1086/452384.
McDonald, R.A., 1995. CORONA-success for space reconnaissance, a look into the cold war, and a revolution for intelligence. Photogramm. J. Remote Sens. 61, 689–720.
Melluma, A., 1994. Metamorphoses of Latvian landscapes during fifty years of soviet rule. GeoJournal 33, 55–62. https://doi.org/10.1007/BF00810136.
Moen, J., Jonsson, B.G., 2003. Edge effects on liverworts and lichens in Forest patches in a mosaic of boreal Forest and wetland. Conserv. Biol. 17, 380–388. https://doi.org/10.1046/j.1523-1739.2003.00406.x.
National Reconnaissance Office, 1967. The KH-4B SYSTEM. National Photographic Interpretation Center (Declassified ed).
Nikodemus, O., Bell, S., Grīne, I., Liepiņš, I., 2005. The impact of economic, social and political factors on the landscape structure of the Vidzeme uplands in Latvia. Landsc. Urban Plan. 70, 57–67. https://doi.org/10.1016/j.landurbplan.2003.10.005.
Nikodemus, O., Bell, S., Penēze, Z., Krūze, I., 2010. The influence of European Union single area payments and less favoured area payments on the Latvian landscape. Eur. Countrys. 2, 25–41. https://doi.org/10.2478/v10091-010-0003-7.
Nikodemus, O., Kļaviņš, M., Krišjāne, Z., Zelčs, V. (Eds.), 2018. Latvija. Zeme, daba, tauta, valsts. Latvijas Universitātes Akadēmiskais apgāds, Riga.
Nita, M.D., Munteanu, C., Gutman, G., Abrudan, I.V., Radeloff, V.C., 2018. Widespread forest cutting in the aftermath of world war II captured by broad-scale historical Corona spy satellite photography. Remote Sens. Environ. 204, 322–332. https://doi.org/10.1016/j.rse.2017.10.021.
Olofsson, P., Foody, G.M., Stehman, S.V., Woodcock, C.E., 2013. Making better use of accuracy data in land change studies: estimating accuracy and area and quantifying uncertainty using stratified estimation. Remote Sens. Environ. 129, 122–131.
Olofsson, P., Foody, G.M., Herold, M., Stehman, S.V., Woodcock, C.E., Wulder, M.A., 2014. Good practices for estimating area and assessing accuracy of land change. Remote Sens. Environ. https://doi.org/10.1016/j.rse.2014.02.015.
Penēze, Z., 2009. Latvijas lauku ainavas izmaiņas 20. un 21. gadsimtā: cēloņi, procesi un tendences. Doctoral Dissertation. University of Latvia, Riga.
Potapov, P.V., Turubanova, S.A., Tyukavina, A., Krylov, A.M., McCarty, J.L., Radeloff, V.C., Hansen, M.C., 2015. Eastern Europe's forest cover dynamics from 1985 to 2012 quantified from the full Landsat archive. Remote Sens. Environ. 159, 28–43. https://doi.org/10.1016/j.rse.2014.11.027.
Prishchepov, A., Radeloff, V.C., Baumann, M., Kuemmerle, T., Müller, D., 2012. Effects of institutional changes on land use: agricultural land abandonment during the transition from state-command to market-driven economies in post-soviet Eastern Europe. Environ. Res. Lett. 7, 024021. https://doi.org/10.1088/1748-9326/7/2/024021.
Prishchepov, A., Müller, D., Dubinin, M., Baumann, M., Radeloff, V.C., 2013. Determinants of agricultural land abandonment in post-soviet European Russia. Land Use Policy 30, 873–884. https://doi.org/10.1016/j.landusepol.2012.06.011.
Rendenieks, Z., Nikodemus, O., Brūmelis, G., 2015. Dynamics in forest patterns during times of forest policy changes in Latvia. Eur. J. For. Res. 134, 819–832. https://doi.org/10.1007/s10342-015-0892-0.
Rigina, O., 2003. Detection of boreal forest decline with high-resolution panchromatic satellite imagery. Int. J. Remote Sens. 24, 1895–1912. https://doi.org/10.1080/01431160210154894.
Ruskule, A., Nikodemus, O., Kasparinska, Z., Kasparinskis, R., Brūmelis, G., 2012. Patterns of afforestation on abandoned agriculture land in Latvia. Agrofor. Syst. 85, 215–231. https://doi.org/10.1007/s10457-012-9495-7.
Ruskule, A., Nikodemus, O., Kasparinskis, R., Bell, S., Urtane, I., 2013. The perception of abandoned farmland by local people and experts: landscape value and perspectives on future land use. Landsc. Urban Plan. 115, 49–61. https://doi.org/10.1016/j.landurbplan.2013.03.012.
Ruskule, A., Nikodemus, O., Kasparinskis, R., Pražavoite, D., Bojāre, D., Brūmelis, G., 2016. Soil-vegetation interactions in abandoned farmland within the temperate region of Europe. New For. 47, 587–605. https://doi.org/10.1007/s11056-016-9532-x.
Scollar, I., Galiatsatos, N., Mugnier, C., 2016. Mapping from corona: geometric distortion in kh4 images. Photogramm. Eng. Remote Sens. 82, 7–13.
Shahtahmassebi, A.R., Lin, Y., Lin, L., Atkinson, P.M., Moore, N., Wang, K., He, S., Huang, L., Wu, J., Shen, Z., et al., 2017. Reconstructing historical land cover type and complexity by synergistic use of landsat multispectral scanner and corona. Remote Sens. 9, 682.
Sohn, H.-G., Kim, G.-H., Yom, J.-H., 2004. Mathematical modelling of historical reconnaissance CORONA KH-4B imagery. Photogramm. Rec. 19, 51–66.
Soille, P., Vogt, P., 2009. Morphological segmentation of binary patterns. Pattern Recogn. Lett. 30, 456–459. https://doi.org/10.1016/j.patrec.2008.10.015.
Solanko, L., Tekoniemi, M., 1999. Novgorod and Pskov: Examples of how Economic Policy Can Influence Economic Development. Russ. East Eur. Financ. Tradehttps://doi.org/10.2307/27749474.
Song, D.-X., Huang, C., Sexton, J.O., Channan, S., Feng, M., Townshend, J.R., 2015. Use of Landsat and Corona data for mapping forest cover change from the mid-1960s to 2000s: case studies from the eastern United States and Central Brazil. ISPRS J.

Photogramm. Remote Sens. 103, 81–92.
Tappan, G.G., Hadj, A., Wood, E.C., Lietzow, R.W., 2000. Use of argon, Corona, and Landsat imagery to assess 30 years of land resource changes in west-Central Senegal. Photogramm. Eng. Remote Sens. 66, 727–736.
Tinker, D.B., Resor, C.A.C., Beauvais, G.P., Kipfmueller, K.F., Fernandes, C.I., Baker, W.L., 1998. Watershed analysis of forest fragmentation by clearcuts and roads in a Wyoming forest. Landsc. Ecol. 13, 149–165. https://doi.org/10.1023/A:1007919023983.
Trimble, 2018. Trimble eCognition Developer User Guide for Windows Operating System. Trimble Germany GmbH Munich, Germany.
Turlajs, J., 1998. Zemes lietotāji kolektivizētajā lauksaimniecībā, karte mērogā 1:1 200 000. In: Turlajs, J. (Ed.), Latvijas Vēstures Atlants. Jāņa Sēta, Riga, pp. 61.
Ullman, S., 1979. The interpretation of structure from motion. Proc. R. Soc. Lond. Ser. B Biol. Sci. 203, 405–426.
Vanwambeke, S.O., Meyfroidt, P., Nikodemus, O., 2012. From USSR to EU: 20 years of rural landscape changes in Vidzeme, Latvia. Landsc. Urban Plan. 105, 241–249. https://doi.org/10.1016/j.landurbplan.2011.12.009.
Vogt, P., Riitters, K., 2017. GuidosToolbox: universal digital image object analysis. Eur. J. Remote Sens. 50, 352–361. https://doi.org/10.1080/22797254.2017.1330650.
Wulder, M.A., Loveland, T.R., Roy, D.P., Crawford, C.J., Masek, J.G., Woodcock, C.E., Allen, R.G., Anderson, M.C., Belward, A.S., Cohen, W.B., et al., 2019. Current status of Landsat program, science, and applications. Remote Sens. Environ. 225, 127–147.